Materials Science and Engineering B 263 (2021) 114859

Contents lists available at ScienceDirect

Materials Science & Engineering B

journal homepage: www.elsevier.com/locate/mseb

Properties of DNA-CTMA monolayers obtained by Langmuir-Blodgett technique

Aleksandra Radko [a], Jacek Nizioł [b,*], Katarzyna Makyła-Juzak [c], Robert Ekiert [d], Natalia Górska [c], Andrzej Górecki [d], Monika Marzec [a]

[a] Institute of Physics, Jagiellonian University, Łojasiewicza 11, 30-348 Kraków, Poland
[b] AGH University of Science and Technology, Faculty of Physics and Applied Computer Science, Mickiewicza 30, 30-059 Kraków, Poland
[c] Faculty of Chemistry, Jagiellonian University, Gronostajowa 2, 30-387 Kraków, Poland
[d] Faculty of Biochemistry, Biophysics and Biotechnology, Jagiellonian University, Gronostajowa 7, 30-387 Kraków, Poland

ARTICLE INFO

Keywords:
Deoxyribonucleic acid
DNA-CTMA complex
Organic electronics
Self-assembly
Thin films
Langmuir-Blodgett technique

ABSTRACT

The complex consisting of DNA and cetyltrimethylammonium chloride (DNA-CTMA) is extensively exploited in organic electronics in form of thin films with submicron or nanometer thickness. In this work, using the Langmuir-Blodgett technique, the surface films were prepared from complexes based on different types of chromosomal and plasmid DNA. The research focused on changes in their continuity after they were transferred onto a solid substrate. It was found that only the monolayer of plasmid DNA-CTMA complex remained continuous after being transferred. The other complexes underwent a spontaneous self-assembling and created elongated linear patterns. AFM images of these patterns were analysed quantitatively with Fast Fourier Transform. It was confirmed that self-assembling occurred along one privileged direction.

1. Introduction

Deoxyribonucleic acid (DNA), carrying genetic information, is the key macromolecule for all living organisms. The physical and chemical properties of DNA have their source in the adopted structure of the double stranded helix (dsDNA). This unique feature makes DNA very different from synthetic polymers and attracts research interests for this macromolecule also in the fields outside life sciences.

DNA has already been proved to be a promising material for applications in areas such as organic electronics, optoelectronics, nonlinear optics or detectors for various chemicals. Comprehensive summary of these innovative ideas can be found in recent reviews, for example [1] – single DNA macromolecules, [2] – DNA nanostructures built from arranged macromolecules (so-called DNA origami) and [3,4] – DNA applied as bulk material in organic electronics.

DNA as the bulk material can be used either in its natural form or, more preferably, in complex with an amphiphilic surfactant [5]. Manipulation of natural DNA encounters many difficulties because it is soluble only in water [6]. In contrast, complexes of DNA and long chain surfactants are insoluble in water. Instead, they are well soluble in a number of alcohols and some volatile non-polar solvents. As a result this derivative is more convenient to handle and can be easily processed, particularly in the form of thin films [7]. The surfactant, most commonly combined with DNA for applications in devices is cetyltrimethylammonium chloride (CTMA) [3]. CTMA molecules bind to DNA [8,9] through ion exchange reaction. This latter can be readily run by mixing aqueous solutions of anionic DNA and cationic CTMA. DNA is a highly hydrophilic biopolymer [10–12], quite the opposite to DNA complexes, in which surfactants significantly reduce the number of sites available for hydration [13–16]. In general, DNA in complex with surfactants seems to preserve its fundamental characteristics, like double helix structure [17,18], optical absorption [19] or thermal resistance [20,21].

Thin DNA-CTMA films have been incorporated as intermediate layers in many optoelectronic devices [22–24]. They are also particularly efficient hosts to be intercalated with various dyes, what makes them particularly exploited in nonlinear optics [25], lasers technology [26] and electrochromic devices [27]. Typically DNA-CTMA is processed into thin films through solution based techniques (ink-jet printing, Dr Blade, dip-coating or, the most often, spin-coating). However, the use of such techniques involves a high loss of material. This is a considerable inconvenience due to the high cost of good quality DNA.

* Corresponding author.
E-mail address: niziol@agh.edu.pl (J. Nizioł).

https://doi.org/10.1016/j.mseb.2020.114859
Received 25 May 2020; Received in revised form 11 September 2020; Accepted 1 October 2020
Available online 16 October 2020

The DNA macromolecule has high aspect ratio with a diameter of 2 nm and a typical length measured in tens of micrometers, what makes it a very promising building material for self-assembled structures on supramolecular level. Such structures can serve as templates to arrange other nano-objects in an organized way. For example, clusters of different metal atoms like silver and gold [28], copper [29] or platinum [30] were arranged in such DNA scaffolds. Tightly arranged clusters, are roughly metallic nanowires with ohmic electronic conductivity [31]. Not only conductive objects can be arranged in this way. Among the others, self-assembled clusters of DNA-mediated TiO_2 nanoparticles were synthesized for photovoltaic application and supercapacitors [32].

Currently, at the nano-scale, single DNA macromolecules can be arranged in a controlled and repetitive manner, but necessary tools are sophisticated and neither cost effective nor time saving. Such an approach is ineffective if micrometer or sub-milimeter size patterns are to be made. In this case less demanding and more productive methods are necessary. Surface patterns can be engraved by standard lithography [33] or written with electron beam [34] on thin solid films from DNA derivatives deposited on a substrate.

The use of DNA in solution or suspension is an optional approach to create patterns on a solid surface. For example by spontaneous, thermodynamically driven pattern formation due to phase segregation. It occurred as a result of drying of an aqueous solution containing DNA and silica nanoparticles was reported [35]. DNA (or derivatives) can be effectively transferred by an intermediating, already pre-patterned, support. It was demonstrated that DNA molecules adsorbed on the stamp, made of elastomeric polydimethylsiloxane (PDMS), can be deposited on a target surface achieving sub-micron resolution [36]. However, a perfect reproduction of such a pattern is strongly limited by irregular inking of the stamp. The reasons are multiple, among the others, the opposite chemical nature of PDMS which is hydrophobic while DNA is mostly hydrophilic and the uncontrolled drying of the deposited solution [37].

Linear grids or dot arrays were obtained via a mould of polymethyl metacrylate (PMMA) and replicated on a glass slide [38]. DNA deposits with submicrometer morphology can be produced by solution micromolding in capillaries on a support surface. Simple solution chemistry allows to control the morphology of the created pattern [39]. Applications of patterned DNA deposited on a surface can be multiple like for example guides for nanoparticle assembling [40].

An interesting alternative way to obtain self-assembling patterns from DNA derivatives is based on Langmuir-Blodgett (LB) technique. This two-step method is straightforward and has no side effects, that the material can be wasted for. A solution of the tested material, in an amount ensuring formation of the monolayer is spread on water surface and compressed to constant value of surface pressure (1st step), then transferred vertically onto solid support (2nd step). As soon as the monolayers were transferred on the mica support, a kind of self-assembling linear patterns appeared spontaneously [41]. We demonstrated that such organized structures can be controlled by the appropriate selection of experimental conditions. The latter concerns in particular the surface pressure, that was pointed out as the key parameter for the physicochemical properties of DNA-CTMA monolayers at the air/water interface.

Further in-depth examination requires an answer whether the observed phenomenon is characteristic only for a given batch of DNA and experimental conditions, or whether it is a more general feature. Biological studies have shown that pDNA is delivered to cells more efficiently than linear DNA. Plasmid DNA is compacted, retaining a significant number of counterions in its vicinity. This in turn drives to a lower effective negative charge [42] that explain why, cationic lipid-mediated delivery of plasmid DNA (pDNA) is better than that of linear DNA in gene therapy. Many other significant differences between chromosomal and plasmid DNA in terms of their activity in the surroundings have also been confirmed. Therefore, in the current work, we investigated the effect of the type of DNA as well as its length on the surface properties of the Langmuir monolayers deposited on mica and silicon substrates.

At the same time, we hoped to find such a DNA that, in the CTMA complex, could be transferred onto a solid substrate in the form of LB monolayer and maintain its continuity. If it were possible, it would open up a cost-effective alternative to spin-coating.

We studied chromosomal DNA of three different lengths and one plasmid DNA. DNA in an eukaryotic cell locates in the nucleus containing double stranded helices packed into chromosomes. In a prokaryotic cells the bacterial circular chromosome is much simpler and often accompanied by the extrachromosomal DNA, called plasmid DNA (pDNA). In contrast to chromosomal DNA, population of pDNA consists of identical macromolecules [43,44]. The pDNA may occur either in linear, circular or supercoiled form, while eukaryotic chromosomal dsDNA adopts typically the linear form [45]. Various biological research indicate differences between plasmid and chromosomal DNA regarding characteristics observed in microscale. Usually, chromosomal DNA is poorly defined in terms of molecular weight distribution. Conversely, this problem does not exist for pDNA. However, so far, the majority of the experiments aimed at technological application were carried out using cheaper and commercially available chromosomal DNA [45] because large amounts of these macromolecules were needed.

2. Materials and methods

2.1. Deoxyribonucleic acid

There were four different types of DNA used. Low molecular weight DNA (dsDNA(*short*)), was purchased from SIGMA Aldrich, while high molecular weight DNA (dsDNA(*long*)) was obtained from CIST (Chitose Institute of Science and Technology, Japan). The latter was extracted from salmon sperm and is often used in research on organic electronics or photonics. Both dsDNA(*short*) and dsDNA(*long*) were further used as delivered.

A portion of dsDNA(*long*) was subjected to ion exchange chromatography in view to elute fraction consisting of shorter and more homogenously distributed molecular masses dsDNA(*chrom*). Ion exchange chromatography was performed in single step at room temperature on ÄKTA Purifier 10 liquid chromatography system. The system was equipped with commercial MonoQ HR10/10 anion exchanger column (Amersham Pharmacia Biotech, Sweden) known for its very high capacity and resolution. 50 mL of DNA solution (at 5 mg/mL) was loaded on the chromatographic column previously equilibrated with A1 buffer (100 mM TRIS, pH 8.0). The separation was carried out with a flow rate of 2.5 mL/min using a sodium chloride gradient over a concentration range up to 1 M NaCl. The gradient length was 3.5 column bed volumes. Optical absorbance at 260 nm and conductivity were monitored during the chromatographic procedure. The DNA fraction appearing in the electrophoregram at conductivity between 57 and 70 mS/cm was selected for further study.

Plasmid DNA (pDNA) was extracted from transformed *Escherichia coli* bacteria grown and harvested in the laboratory. *E. coli* bacteria transformed with phMGFP plasmid was grown at standard LB medium with the addition of 0.1 mg/mL ampicillin. The bacteria were streaked on solid LB medium at Petri dish and incubated overnight at 37 °C. The single colony was transferred into 30 mL liquid LB medium and shaked vigorously overnight. 10 mL of this culture was transferred to 1 L of liquid LB medium and shaked overnight at 37 °C. Bacteria were pelleted by centrifugation (7000 g, 30 min) and the plasmid DNA purified using the NucleoBond PC 10000EF Giga KIT from Macherey-Nagel GmbH&Co according to the manufacturer's instructions. The obtained DNA was tested using UV–Vis spectroscopy (to determine its purity and concentration) and electrophoresis (in order to determine the length of the DNA).

Each of the four different DNAs batch was converted into complex with cetyltrimethylammonium chloride (CTMA). The synthesis started

by preparing equimolar solution of DNA and CTMA. Then the CTMA solution was dropwise added to DNA solution constantly stirred with a magnetic bar. The received precipitate was filtered at Büchnel funnel, washed excessively with water and freeze-dried. Next it was dissolved in a spectroscopic grade ethanol and later spectroscopic grade chloroform was added to obtain 4:1 v/v mixture. A volatile solvent was required in Langmuir experiments.

Other chemicals like tris(hydroxymethyl)aminomethane (Tris base), hydrochloric acid (HCl) and CTMA (>98%) were purchased from SIGMA-Aldrich while organic solvents such as ethanol, chloroform or acetone of analytical grade were delivered by POCH (Poland).

2.2. Electrophoresis

With a view to spatially separate macromolecules of different molecular mass, the studied DNA samples were subjected in aliquots to electrophoresis in 3.5% (w/v) agarose (for dsDNA(short) and dsDNA (*chrom*)) or 2% (w/v) agarose (for dsDNA(*long*) and pDNA) gel in TBE buffer according to standard procedure using Mupid-exU apparatus. The processed DNA was stained with ethidium bromide and visualized in UV-light.

2.3. FTIR measurements

Fourier transform middle-infrared absorption measurements (FT-MIR) were performed at room temperature using a Bruker VERTEX 70v vacuum spectrometer. The spectra were obtained in the spectral range of 400–4000 cm^{-1} with a resolution of 2 cm^{-1} and 32 scans per each spectrum. Four bulk samples of DNA-CTMA complex, prepared using different types of DNA (low molecular weight, high molecular weight, short and plasmid), were mixed with KBr, compressed into pellets, and then measured.

2.4. Langmuir monolayer technique

The surface pressure–area (π–A) isotherm was recorded by using a two-barrier Langmuir trough (NIMA) of 503 cm^2 total area. Surface pressure was measured with accuracy of ± 0.1 mN m^{-1} using a Wilhelmy plate made of ashless chromatography paper (Whatman). Before measurement, water subphase was cleaned by closing the barrier and aspirating water until surface pressure readings were not exceeding ± 0.1 mN m^{-1}, in comparison with values of surface pressure detected with the opened barriers. The subphase temperature was controlled thermostatically, by a circulating water system (Julabo), and kept at 20 °C ± 0.1 °C. Spreading solution was deposited drop by drop onto the water subphase with a 250 μl Hamilton microsyringe, precise to 5.0 μl. After spreading, monolayer was left to equilibrate for 5 min and then compressed with barrier speed of 20 cm^2 min^{-1}. Recorded π-A isotherm was repeated at least twice to ensure high reproducibility of the results.

In order to complement the interpretation of the results, the morphology of examined monolayer was studied with Brewster angle microscope (BAM) (Accurion GmbH, Germany), equipped with a 50 mW laser emitting p-polarized light at a wavelength of 658 nm and an objective with tenfold magnification. The microscope was installed over a KSV NIMA Langmuir trough (Finland) with two barriers and 841 cm^2 of its total area.

2.5. Langmuir- Blodgett deposition technique

A series of preliminary control experiments were conducted on dsDNA(short)-CTMA to investigate the effect of various factors on surface film formation. We observed that $\pi - A$ isotherms did not depend neither on varied number of molecules deposited on the surface nor on the temperature of the experiment (10–30 °C). Furthermore, even different monolayer speed compression (10–30 mm/min), had no significant impact on the characteristics of dsDNA(short)-CTMA surface film. In order to adjust the most favorable conditions for the monolayer transfer on solid support, the static stability experiment was performed. The dsDNA(short)-CTMA monolayer was compressed until the chosen surface pressure (5, 10, 15 and 20 mN/m), kept constant afterwards. Simultaneously, the decreasing area was monitored as a function of time. It occurred that dsDNA(short)-CTMA film was the most stable when compressed up to 15 mN/m.

Langmuir monolayers were transferred onto mica and silica substrates, using Langmuir- Blodgett deposition technique (LB technique). Before each experiment, solid substrate was placed in a water subphase. After spreading solution of DNA-CTMA complex onto a water subphase, the monolayer was left to equilibrate for 5 min and then compressed to constant value of surface pressure of 15 mN/m. LB deposition was carried out by lifting-off the solid substrate from the water subphase through the monolayer with a dipper speed of 5 mm per minute. The substrates were either ruby muscovite mica sheets of V1 quality purchased from Continental Trade (China) or silica wafers obtained from ITME (Poland). Immediately before LB experiments the substrate surface was cleaned - mica's with adhesive tape while silicon plate's in ultrasonic baths for 15 min both in acetone and ethanol, then treated with plasma for 30 s.

2.6. Atomic Force Microscopy (AFM) imaging

Atomic Force Microscopy profiling was done in non-contact mode. Images were obtained at room temperature using Agilent 5500 Microscope at resonance frequency of 45–115 Hz. Nanosensor tips of PPP-FMR-50 type and thickness of 3.0 ± 1 μm were used. For each layer, topography images were collected from several, randomly chosen, areas and images were acquired with 256 × 256 lines. Set-point and gains were adjusted to each measurement in order to obtain a clear, noiseless image. The scan rate was determined individually and ranged from 0.9 to 1.3 lines s-1. The background of the images was removed by flattening algorithm, and the contrast and brightness were adjusted using the Gwyddion 2.47 software. The AFM images presented are 2.5 μm × 2.5 μm in size and are representative scans for each DNA type complex. Depth profiles provided by AFM were analyzed using Fast Fourier Transform (FFT) algorithm embedded in OriginPRO 2019 software package.

2.7. Water contact angle measurements

Static contact angle measurements were performed at room temperature by the sessile drop technique using a Kruss EasyDrop (DSA15) instrument. The contact angle values are obtained by averaging the measurements of five different drops and the error was calculated as standard deviation.

3. Results and discussion

3.1. Estimation of DNA molecular mass distribution

Deoxyribonucleic acid extracted from bacterial cell culture (pDNA) is a monodisperse biopolymer with a well-defined molecular weight. Unfortunately, this method does not allow large quantities to be obtained. However, for applications in technology, one would need a cost-effective DNA. The latter in large quantities is obtained from various bulk natural resources (often biological waste). In contrast to bacterial DNA, such a material is characterized by a statistical mass distribution.

In our study only pDNA as derived from *E.coli* bacteria was supposed to have monodispersed molecular mass, given by the supplier as 4707 bp (the number of base pairs is directly related to the molecular mass as $1bp = 660gmol^{-1}$). Somehow, the mass distribution of other types of DNA should be determined. Standard techniques used for synthetic polymers such as gel permeation chromatography (GPC) or high-

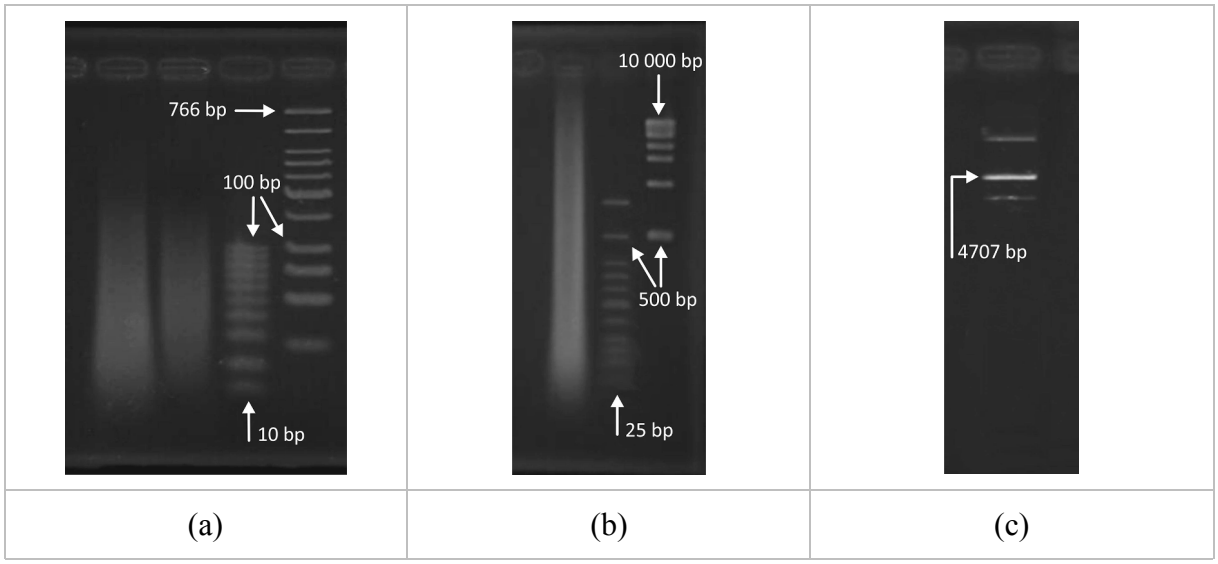

Fig. 1. (a) from left to right – dsDNA(*short*), dsDNA(*chrom*), 10 bp and LMW ladders, (b) from left to right – dsDNA(*long*), LMW and 1kbp ladders, (c) pDNA.

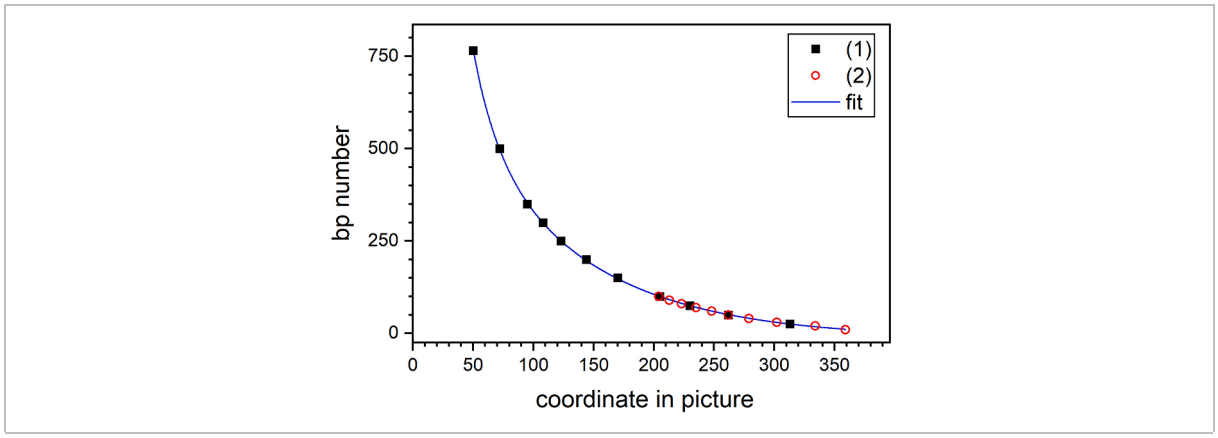

Fig. 2. An example, data expressing position in the gel (from Fig. 1(a)) are calibrated in bp units. (1),(2) – steps of LMW and 10 bp ladders, respectively. LMW ladder consists DNA of 766, 500, 350, 300, 250, 200, 150, 100, 75, 50 and 25 bp, while 10 bp ladder DNA of 100, 90, 80, 70, 60, 50, 40, 30, 20 and 10 bp. Solid line represents double exponential decay fit.

pressure liquid chromatography (HPLC) are useless in the case of DNA for many reasons, like for example inadequacy of reference standards or inherent properties of DNA as polyelectrolyte.

We decided to derive indirectly the necessary data from gel electrophoresis, the well-established technique for DNA mass separation. In this technique a portion of DNA sample is injected in agarose gel plate, then travels along applied electric field. The speed depends inversely on molecular mass. Finally, the gel is stained with a UV fluorescent dye, that is retained exclusively in the DNA double helix. The reference sample, (the so-called DNA ladder consisting of macromolecules of several, well-defined masses) is simultaneously injected. Finally, the gel with mass separated DNA is imaged in UV light, with the tonal span adjusted so that it falls within the linear region of the dynamic response of the camera. At the first approximation the dye content in a particular place of the gel may be considered proportional to the number of base pairs available there, i.e. the quantity of DNA accumulated. Thus, the recorded fluorescence intensity can be directly related to. The distance travelled from the injection point (well) can be recalculated in bp numbers using the DNA ladders step positions. In our study we used 1 kb DNA Ladder and Low Molecular Weight (LMW) DNA ladder both from New England BioLabs Inc. and 10 bp DNA Step Ladder from Promega Co.

In Fig. 1 are shown images of three stained gels containing separated DNA (that can be observed in form of stripes) with calibration ladders. For dsDNA(*short*) and dsDNA(*chrom*) a different calibration was used than for dsDNA(*long*), so they are shown separately, respectively in Fig. 1(a) and (b). Fig. 1(c) shows an image of a pDNA sample, which consists of three bands instead of one, as might have been expected, one corresponding to 4707 bp. This fact indicates that pDNA adopts also forms other than linear (i.e. circular and supercoiled).

Fig. 2 shows an example of the dependence between the ladder step positions and the corresponding bp number. This dependence fits perfectly with a double exponential decay function, that was later used to convert coordinate of the position occupied by a DNA fraction to its molecular mass in bp. While there are arguments for choosing such a function, they are beyond the scope of the reported research. Therefore, for our purpose, this function only shows a smooth curve through the experimental points.

Fig. 3 illustrates how one can deduce molecular mass distribution of the studied DNA samples using data provided by gel electrophoresis. At first, the fluorescence intensity of stripes, derived from images, is represented as function of the position in the gel (Fig. 3(a)). Then, the abscissa is recalculated to bp as in Fig. 3(b). However, it should be stressed, that such a conversion should not be done outside mass span covered by reference ladders. It is especially true for the high mass end, where

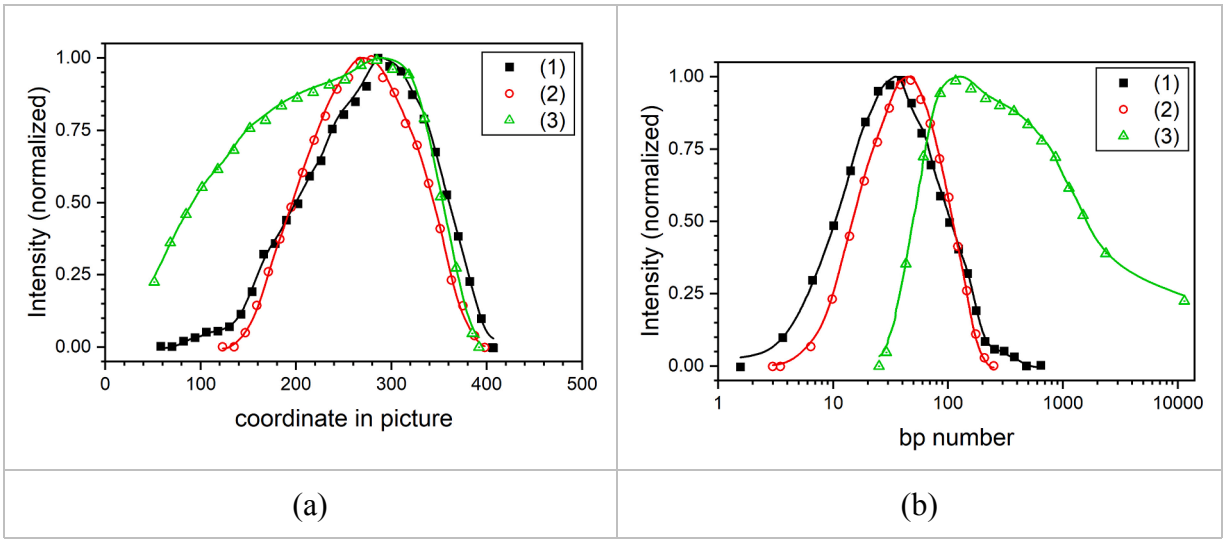

Fig. 3. Fluorescence intensities of the studied DNA stripes from Fig. 1(a) and (b), normalized to their maxima: (a) intensity dependence on the position in the picture, (b) intensity dependence on bp number (note the logarithmic scale). Plots (1), (2) and (3) represents data for dsDNA(*short*) dsDNA(*chrom*) and dsDNA(*long*), respectively.

Table 1
Characteristics of molecular mass distribution deduced from electrophoresis results.

sample	Molecular mass range [bp]	M_n[*bp*]	M_w[*bp*]
dsDNA(*short*)	5–240	82	117
dsDNA(*chrom*)	6–190	75	97
dsDNA(*long*)	25–10000	4200	6500
pDNA*	4707	–	–

(*) molecular mass for *p*DNA as stated by the supplier.

conversion function rises very fast and therefore the uncertainty of the result is high. For this reason, dsDNA(*long*) data was cut out at 10 000 bp, and the final result is a rather lower estimate of the true value. Finally, number average (M_n) and weighted average (M_w) molar masses are obtained by numerical integration, according to their definitions. The result are summarized in Table 1.

The data in Table 1 as well as Fig. 3(a) prove that ion exchange chromatography significantly reduced the molecular mass of dsDNA (*long*). The achieved span of the molecular mass was similar to natural dsDNA(*short*). However, in contrast to the latter, dsDNA(*chrom*) was deprived of higher mass tail, which is the origin of less substantial difference between M_n and M_w.

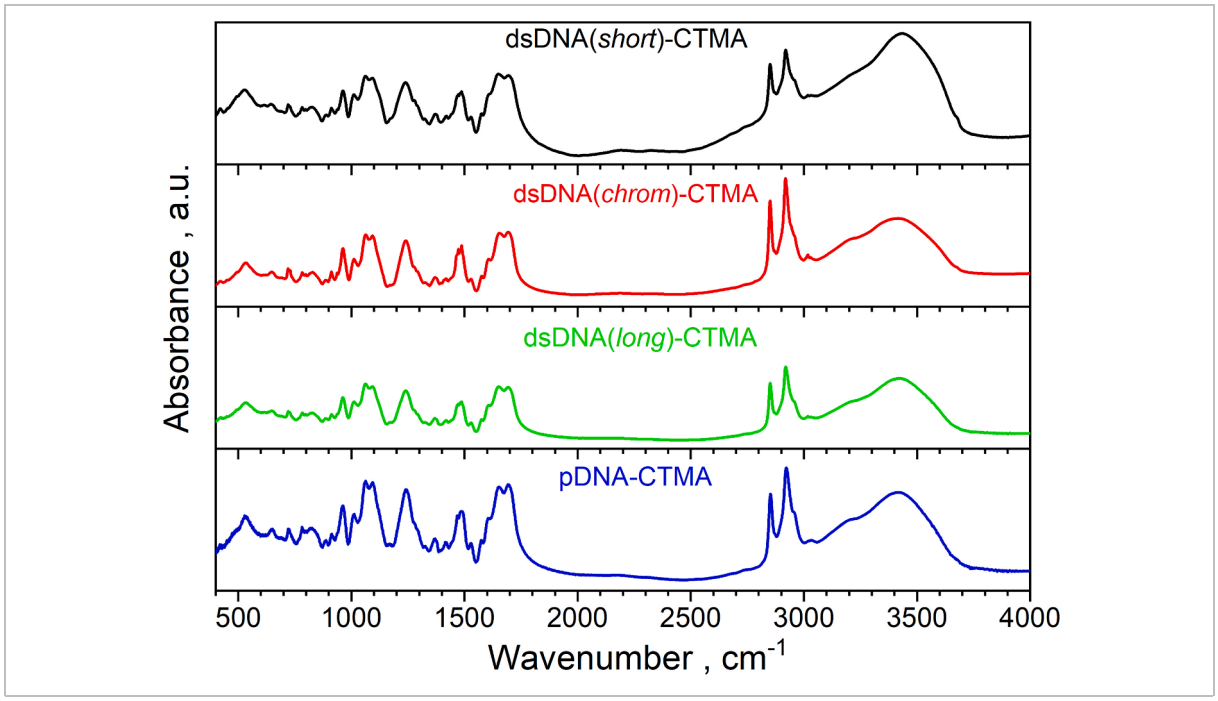

Fig. 4. Comparison of FT-IR spectra of the DNA-CTMA complex synthesized using four different types of DNA.

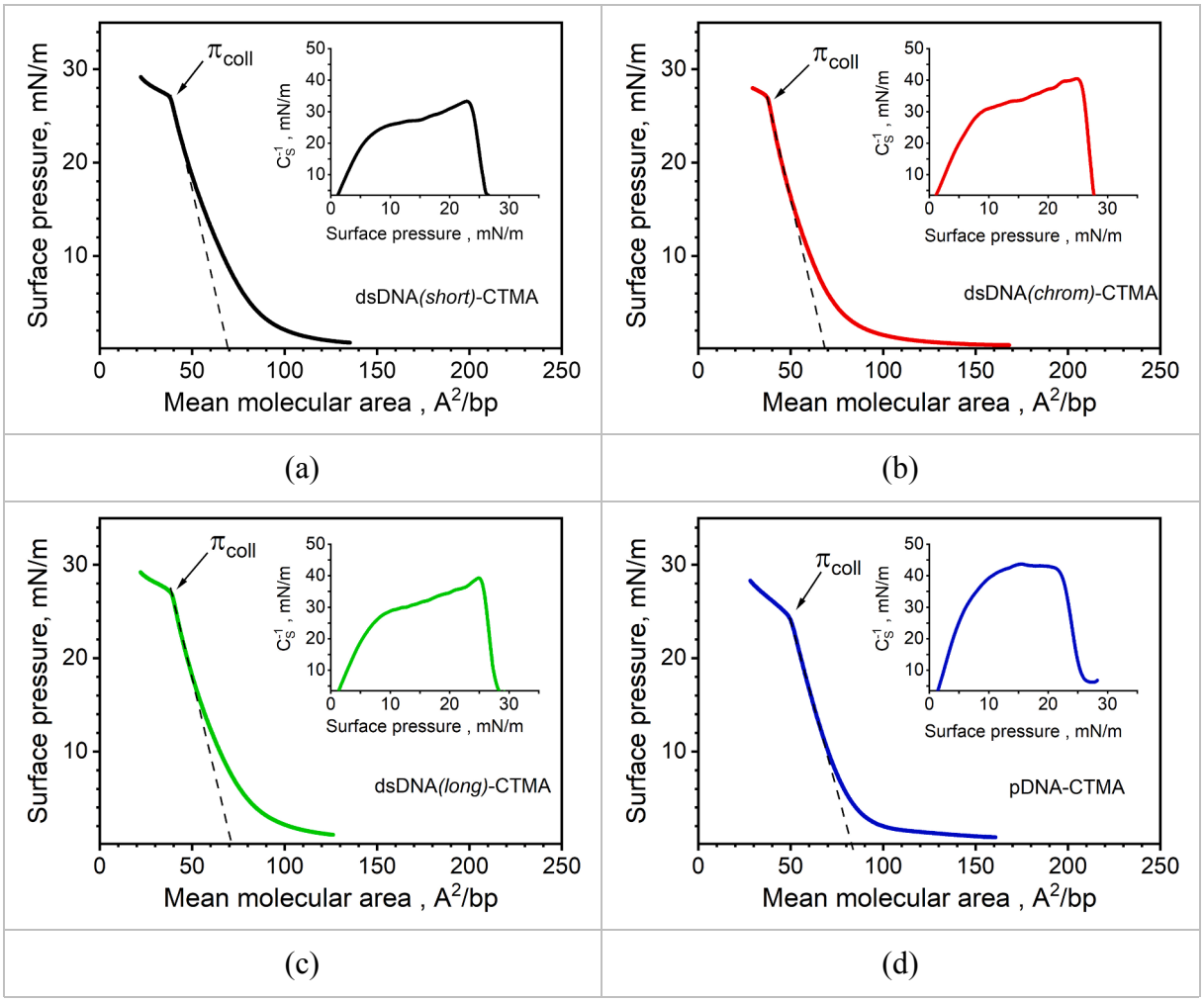

Fig. 5. The surface pressure–area (π–A) isotherms registered for different complexes: (a) dsDNA(*short*)-CTMA, (b) dsDNA(*chrom*)-CTMA, (c) dsDNA(*long*)-CTMA, (d) pDNA-CTMA spread on water subphase at 20 °C. Insets: compression moduli as a function of surface pressure.

3.2. FTIR measurements

Infrared absorption spectra of four reaction products consisting of different types of DNA were measured to determine whether conversion to the DNA-CTMA complex had actually occurred and to detect possibly existing molecular or structural differences between them (Fig. 4). Indeed, all these spectra are very different from the spectrum obtained for a physical mixture of DNA and CTMA [41] and thus confirm the creation of DNA-CTMA complexes. In particular, comparing to the spectra of pure DNA and CTMA, some modifications can be observed. The bands resulting from $\nu_{as}(CH_2)$ and $\nu_s(CH_2)$ stretching vibrations of hydrocarbon chains are shifted to larger wavenumbers, which suggests slightly less ordered hydrocarbon chains of CTMA as the result of electrostatically binding to the phosphate backbones of DNA. In the spectral range where the in-plane stretching vibration related to cytosine-guanine pairs occurs, a band observed at 1536 cm^{-1} in pure DNA is shifted toward smaller wavenumbers by about 8 cm^{-1} and additionally a new band at 1575 cm^{-1} appears in the spectra of all DNA-CTMA complexes. In turn, the band particularly sensitive to a cationic surfactant binding to DNA is connected to the $\nu_{as}(PO_2^-)$ vibration observed at 1228 cm^{-1} in pure DNA. In the case of all four complexes this band is shifted by about 13 cm^{-1} towards larger wavenumbers and is of distinctly larger intensity. In the low wavenumber range (below 900 cm^{-1}) some changes are also noticeable. The band, which is a deoxyribose-phosphate backbone marker of B-form DNA, observed at 832 cm^{-1} in pure DNA, is shifted toward smaller wavenumbers by about 5 cm^{-1} whereas two bands at 641 and 533 cm^{-1} in pure DNA are shifted toward larger wavenumbers by 8 and 7 cm^{-1}, respectively, in case of all the DNA-complexes.

What is important, the spectra obtained for all four DNA-CTMA complexes, differing in the type of DNA used in their syntheses, are essentially very similar taking into consideration shapes, positions and intensities of all bands. The only visible difference that can be distinguished is for plasmid DNA-CTMA complex, where $\nu_{as}(CH_2)$ and $\nu_s(CH_2)$ stretching bands are slightly shifted toward larger wavenumbers by about 3 and 2 cm^{-1}, respectively, comparing to the spectra of the other three complexes. It may indicate slightly less ordered hydrocarbon chains of CTMA ligands around DNA strands in the plasmid DNA complex.

3.3. Langmuir monolayer technique

Fig. 5(a–d) presents the surface pressure–area (π–A) isotherms registered for different complexes of dsDNA-CTMA as well as pDNA-CTMA. For each examined monolayer a similar course of registered (π–A) isotherm is observed. With the decreasing area, the surface pressure rises very slowly and the slope smoothly becomes steeper. As the compression progresses, a significant rise in the surface pressure is observed, however, without any noticeable phase transition, until the film collapses (at about $27 mN \cdot m^{-1}$ for dsDNA-CTMA and $24 mN \cdot m^{-1}$ for pDNA-CTMA).

Additionally, in order to characterize the physical state of each

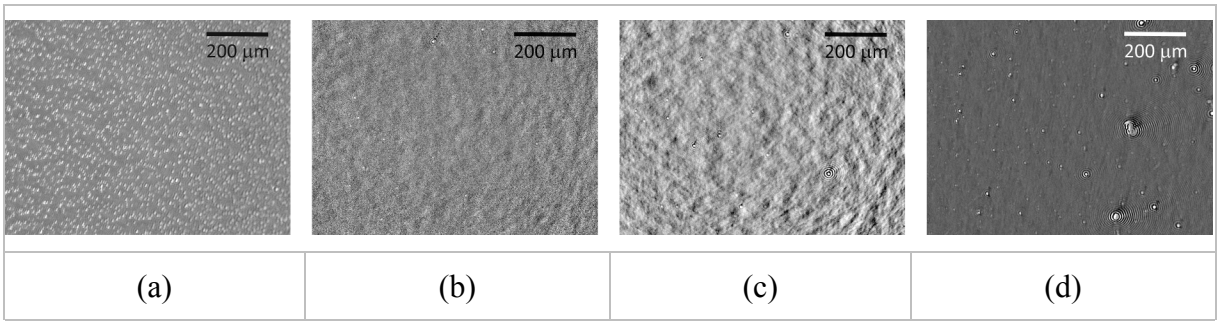

Fig. 6. BAM images recorded during the compression for different complexes: (a) dsDNA(*short*)-CTMA, (b) dsDNA(*chrom*)-CTMA, (c) dsDNA(*long*)-CTMA, (d) *p*DNA-CTMA. These textures were observed at the values of collapse pressure (π_{coll}) indicated in Fig. 3(a–d).

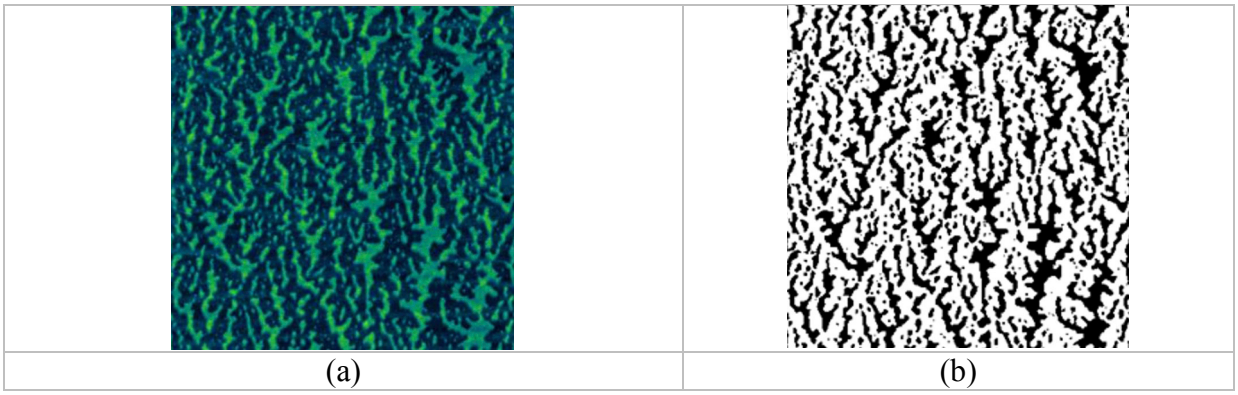

Fig. 7. SCR calculation procedure: (a) original AFM image, (b) uncovered regions marked in black.

Langmuir monolayer, the compression moduli (defined as $C_S^{-1} = -A(\partial\pi/\partial A)_T$, A denotes average area per base pairs in a monolayer) values were calculated from the isotherm data set and plotted as a function of surface pressure in the inset in Fig. 5. According to the physical state classification based on C_S^{-1} values [46], it is evident that each investigated DNA-CTMA complex forms liquid-type monolayer. As one can see Fig. 5(a–c), characteristics obtained for each chromosomal DNA are almost identical. Extrapolating the rectilinear fragment of the (π–A) isotherm (i.e. the last rectilinear part of the isotherm, recorded at high surface pressure values) to $\pi = 0$, the value of the limiting area A_{lim} is obtained. In other words, A_{lim} can be defined as the area occupied by the base pairs, at the largest packing of molecules in monolayer [47,48]. Estimated values of limiting area for dsDNA-CTMA complexes are $71.3 \pm 0.2\,\text{Å}^2/bp$; $68.9 \pm 0.2\,\text{Å}^2/bp$, $71.2 \pm 0.1\,\text{Å}^2/bp$ for dsDNA(short)-CTMA, dsDNA(chrom)-CTMA and dsDNA(long)-CTMA respectively, while for pDNA-CTMA is slightly larger and equals $83.4 \pm 0.1\,\text{Å}^2/bp$. The difference may be due to the diverse structures of plasmid DNA macromolecules in comparison to chromosomal DNA. Plasmid DNA is a circular form of DNA that at physiological pH may adopt a supercoiled conformation depending on the ionic strength, while chromosomal DNA fragments, i.e., from salmon sperm, remain in a linear form. Furthermore, supercoiling effect renders a less effective negative charge of the biopolymer than its actual charge [42].

During the compression, the textures of DNA-CTMA films were observed with Brewster Angle Microscopy (BAM). Such a visualization did not reveal any significant variations in the film morphology until it collapsed (at π_{coll}). Regardless the surface pressure, the morphology of the each complex was completely smooth and homogeneous (data not shown). A kind of roughness appeared only at the collapse pressure, as shown in Fig. 6. In the case of pDNA-CTMA monolayer grainy objects appeared, but their origin remained unknown.

The results prove that all investigated DNA-CTMA complexes form stable Langmuir monolayers at the air/water interface. Usually in Langmuir-Blodgett practice, such monolayers when transferred onto a solid surface, provide smooth and flawless films. However, in the current research, the results were partially different.

3.4. AFM imaging and FFT analysis

Based on the recorded AFM images, the surface covering ratio (SCR) was calculated by using the ImageJ software. First, we discriminate in the AFM image (Fig. 7(a)) regions considered as uncovered substrate (black in Fig. 7(b)). Then, the SCR was calculated as $\text{SCR} = \frac{\text{blackpixell}}{\text{allpixell}} \cdot 100\%$. The uncertainty of this method was in the order of single percent.

The morphology of DNA-CTMA layers deposited on mica and silica substrates are presented in Fig. 8. The images of these layers, obtained by Atomic Force Microscopy (AFM), represent the surface of 2.5 µm by 2.5 µm and the height ranging between 0 and 5 nm. All the samples were prepared under identical experimental conditions: the surface pressure at the moment of lifting 15 mN/m and the dipper speed 5 mm/min. However, a closer visual inspection reveals significant differences between layers deposited on mica and silicon wafers. The vertical arrow on the left side of Fig. 8 indicates the direction of substrate pulling out from the subphase in Langmuir trough. In the case of mica substrate and chromosomal DNA, organized strip-like forms were obtained instead of a homogeneous film. They are clearly aligned along the drawing direction. Monolayers transferred onto silicon substrates disintegrated into statistically distributed grains.

DNA is inherently a polar macromolecule, but the DNA-CTMA complex in aqueous solution exhibits lyotropic liquid crystal (LLC) properties [49]. Two fundamental arrangements were determined. The first is the lamellar phase (L_α) with alternating lipid bilayers and DNA monolayers and the second is the inverted hexagonal phase (H_{II}),

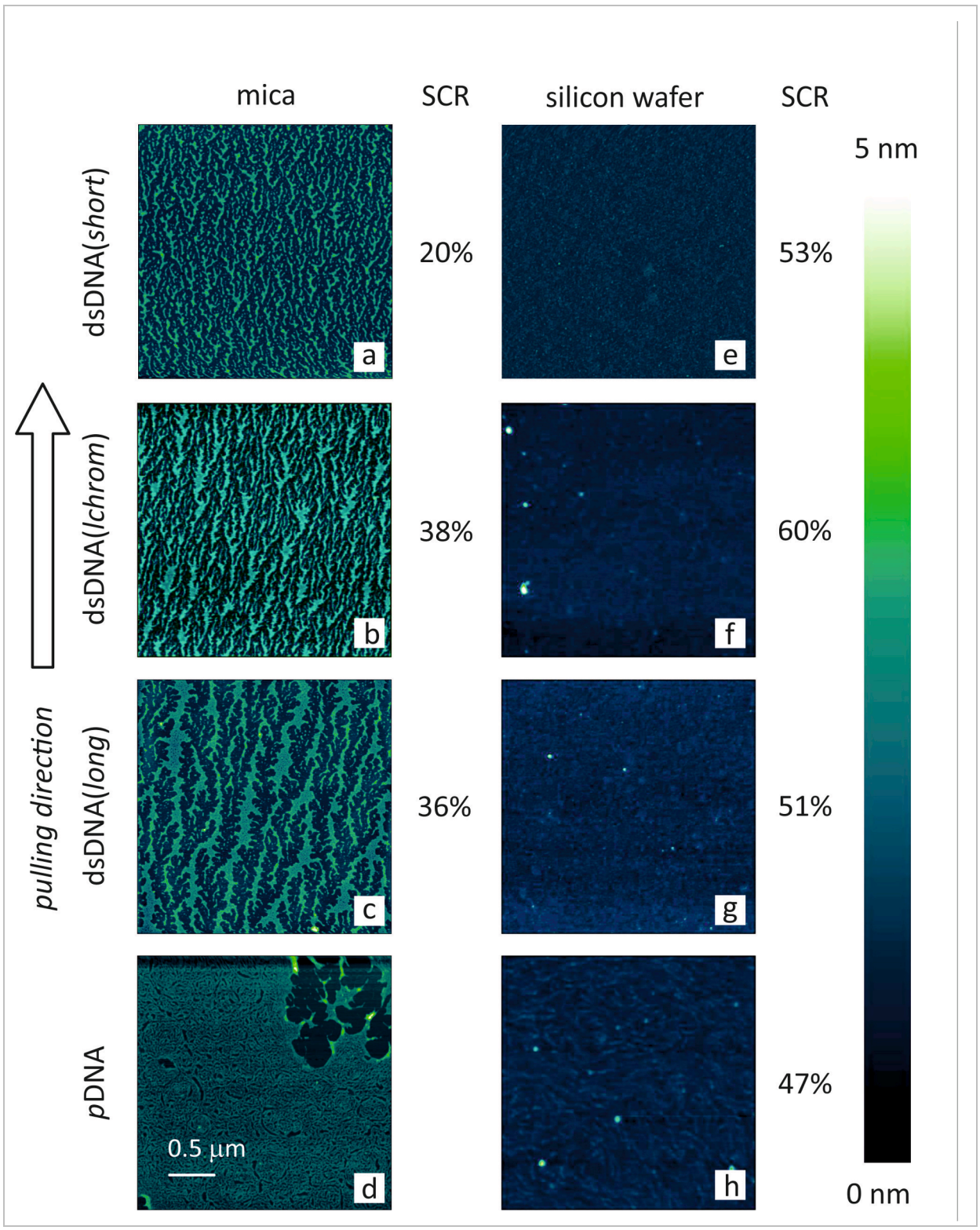

Fig. 8. Topology of DNA-CTMA deposits obtained from monolayers transferred onto either mica or silicon substrates. Images were obtained by AFM microscopy at non-contact mode. Surface covering ratio (SCR) expresses the fraction of surface occupied by DNA complex.

composed of DNA inserted within inverse lipid tubules, which are organized in a hexagonal lattice [49]). Most likely, such an architecture, at least to some extent, is also preserved also in solid form. This means that DNA-CTMA complex is rather hydrophobic, which contrasts with the hydrophilic nature of mica and silicon. The contact angles measured for both substrates used were 17.85 ± 0.27 and 25.55 ± 0.61°for mica and silicon, respectively. Mica plates were freshly cleaved and silicon wafers factory polished, so the roughness factor of both should be negligible and have no significant effect on the formation of layers. Considering the latter, it is surprising that the relatively small difference in surface wettability resulted in such large variations in the observed ordering.

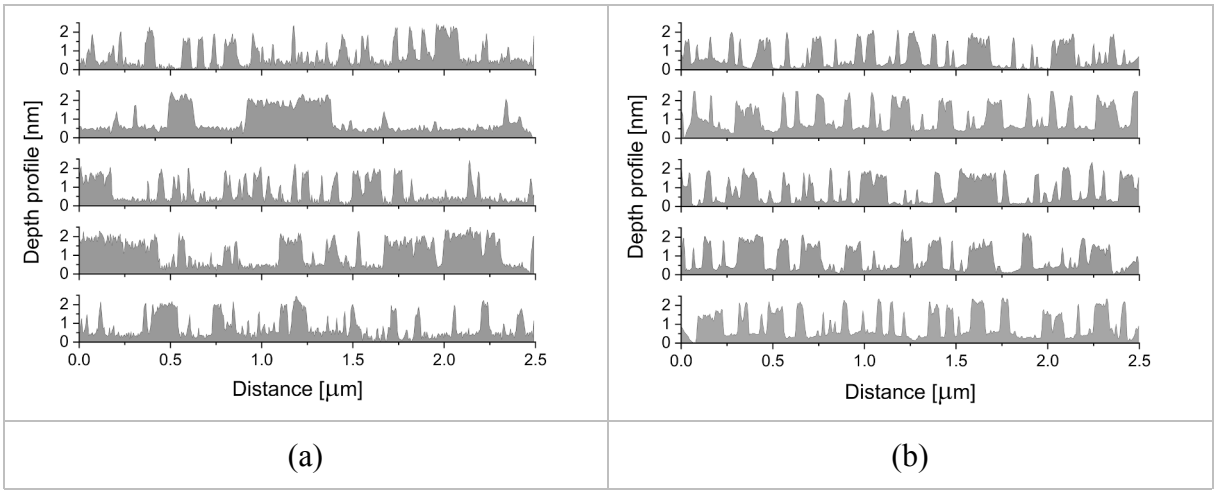

Fig. 9. Examples of depth profiles from dsDNA(*long*) AFM image (Fig. 5) cut (a) in parallel and (b) perpendicularly to the drawing direction.

Apparently, the observed behavior is governed also by other factors (like for example surface free energy) that were not controlled in the reported study. A more precise determination of these factors indicates a possible, further direction of this research. It may turn out that a compatibilizing agent is required for the successful transfer of DNA-CTMA surface films to silicone substrates.

Surprisingly, unlike in the case of chromosomal DNA, the pDNA-CTMA monolayer retained its initial continuity after being transferred onto the mica plate. As one can see in Fig. 7d, such a surface was almost perfectly free of defects, at least at the spatial scale of this analysis. At a larger scale of observation some artifacts in form of randomly distributed holes were spotted in this layer (as evidenced in upper right corner in Fig. 8d). However, very similar artefacts are often found also in various other monolayers and usually they are attributed to contaminations entrapped from the air. At this stage of research, it is difficult to find credible reasons explaining the uniqueness of pDNA compared to chromosomal DNA samples. They are all made up of the same base pairs, which should result in the same chemistry of basic interaction with the surroundings. It can be speculated that the differences observed are due to the distinctly different macrostructures adopted by these macromolecules. Nevertheless, this finding is highly important for practical applications, because it proves that the Langmuir monolayers of DNA-CTMA complex can be successfully transferred on ~~a~~ solid substrates.

To describe the observed patterns in a more quantitative and general manner, we analyzed cross-section profiles drawn in parallel and perpendicularly to the direction that the substrates were pulled out of the water subphase. Examples of such a cross-sections obtained for the AFM image of dsDNA(*long*)-CTMA are sketched in Fig. 9. The visual comparison reveals greater regularity in Fig. 8(b), i.e. for a cross-section cut perpendicularly.

Fast Fourier Transform (FFT) it is a numerical method that can help to detect periodicity in a noisy signal. In this study spatial depth profiles (like these in Fig. 9) were transformed in the wavelength space as it is illustrated in Fig. 10. If in the plot representing the FFT amplitude versus the wavenumber occurs a maximum, it means that the analyzed profile actually contains a periodic pattern. Its characteristic wavelength can be calculated as the inverse of the maximum wavenumber.

Conversely, a monotonic decrease in FFT amplitude towards higher wavenumbers indicates lack of periodicity in the source profile. A closer inspection of experimental data derived for deposits on silicon does not allow any periodicity to be detected. That is, the observed granules are distributed in a completely random manner. In the case of deposits on mica, only the graphs for perpendicular cuts have clearly visible maxima. The latter confirms the presence of a real periodicity in the source pattern and line orientation along the pulling direction. These maxima are located at approximately 10 μm^{-1} and 6 μm^{-1} respectively for shorter and longer DNA as can be seen in lower parts of Fig. 10(a, c, e). In other words, the average spacing between lines obtained from shorter DNA is about 0.1 μm, while the lines of longer DNA are further apart and lie 0.17 μm each from the other. This result clearly indicates that the self-organization of chromosomal DNA in linear patterns is not entirely a random process but depends on the parameters of the material used to form the monolayer.

4. Conclusions

In this work we studied surface properties of DNA-CTMA complex monolayers prepared by Langmuir-Blodgett technique. We outlined problems related to their transfer on a solid support. To our best knowledge it was demonstrated for the first time, that DNA-CTMA complex derived from plasmid DNA is capable to form stable Langmuir monolayers at the air–water interface monolayer by Langmuir-Blodgett technique as well as can be efficiently transferred with Langmuir-Blodgett technique onto a solid support without losing its continuity.

Therefore, it may seem that the use of plasmid DNA will open a new route in organic electronics. Spin coating commonly used in this field as a thin film deposition technique is ineffective due to the generated material losses. In contrast, Langmuir-Blodgett technique is far less material consuming and virtually lossless. The rest of the tested complexes, based on ~~other~~ different chromosomal DNAs, did not meet the challenge. Following the transfer, layers underwent a spontaneous self-organization in linear patterns. Preliminary, cursory observations suggest that this this phenomenon is governed by wettability of the support and the molecular mass of DNA. On the other hand, such linear patterns, useless for organic electronics based on layered architecture, may be advantageous in other applications. For example, they may be used as host templates to arrange metals or small molecules in a similar manner to already reported [50], of course if the quality control of the DNA-CTMA patterns is improved. Such an approach would probably become an interesting alternative to lithographic techniques.

5. Data availability

The raw/processed data required to reproduce these findings cannot be shared at this time as the data also forms part of an ongoing study.

Declaration of Competing Interest

The authors declare that they have no known competing financial

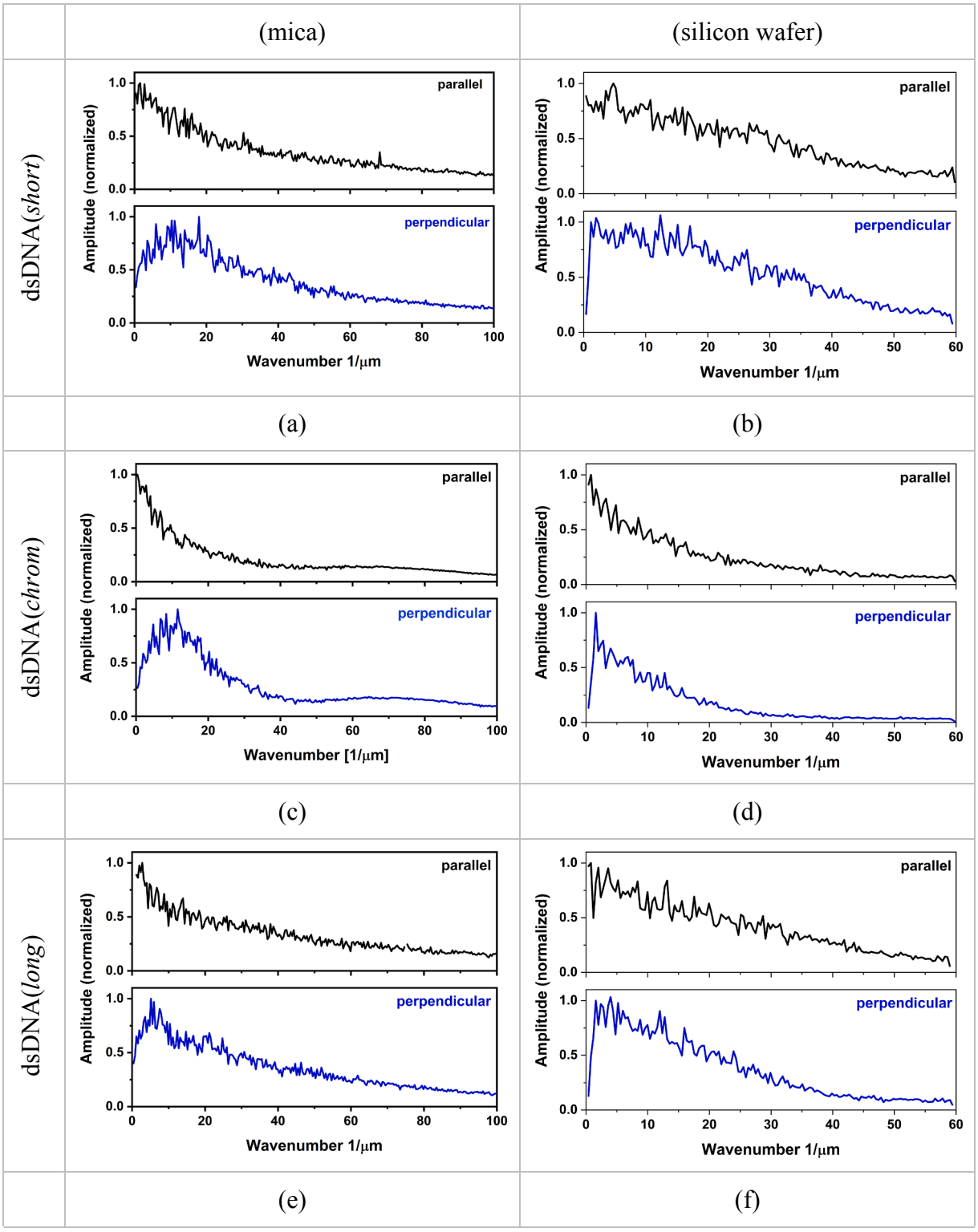

Fig. 10. Results of FFT analysis performed on depth profiles extracted from AFM images for different DNA used on the mica (a, c, e) and silicon (b, d, f) substrates. Each graph is labelled by the cut direction with respect to the drawing direction. Amplitudes were normalized to the maximum.

interests or personal relationships that could have appeared to influence the work reported in this paper.

Acknowledgements

Aleksandra Radko acknowledges financial support of the Ministry of Science and Higher Education in Poland (grant no. 7150/E-338/M/2017).

This research was carried out with the equipment (ultra-BAM) purchased thanks to the financial support of the European Regional Development Fund in the framework of the Polish Innovation Economy Operational Program (Contract No.POIG.02.01.00-12-023/08).

References

[1] K. Wang, J. Funct. Biomater. 9 (2018) 8.
[2] F. Zhang, J. Nangreave, Y. Liu, H. Yan, J. Am. Chem. Soc. 136 (2014) 11198–11211.
[3] E.F. Gomez, A.J. Steckl, Engineering DNA and Nucleobases for Present and Future Device Applications, in: M. Irimia-Vladu, E.D. Glowacki, N.S. Sariciftci, S. Bauer (Eds.) Green Materials for Electronics, Wiley-VCH, 2018, pp. 191-233.
[4] E.F. Gomez, V. Venkatraman, J.G. Grote, A.J. Steckl, Adv. Mater. 27 (2015) 7552–7562.
[5] K. Liu, L. Zheng, C. Ma, R. Göstl, A. Herrmann, Chem. Soc. Rev. 46 (2017) 5147–5172.
[6] W. Saenger, Principles of Nucleic Acid Structure, 1 ed., Springer, 1984.
[7] K. Tanaka, Y. Okahata, J. Am. Chem. Soc. 118 (1996) 10679–10683.
[8] D.-M. Zhu, R.K. Evans, Langmuir 22 (2006) 3735–3743.
[9] R.S. Dias, K. Dawson, M.G. Miguel, in: DNA Interactions with Polymers and Surfactants, John Wiley & Sons, Inc., Hoboken, NJ, USA, 2008, pp. 89–117, https://doi.org/10.1002/9780470286364.ch4.
[10] M. Falk, K.A. Hartman, R.C. Lord, J. Am. Chem. Soc. 84 (1962) 3843–3846.
[11] H. Haranczyk, J. Czak, P. Nowak, J. Niziol, Acta Phys. Polon. A 117 (2010) 397–402.
[12] M.G. Kubinec, D.E. Wemmer, J. Am. Chem. Soc. 114 (1992) 8739–8740.
[13] H. Haranczyk, J. Kobierski, D. Zalitacz, P. Nowak, A. Romanowicz, M. Marzec, J. Niziol, E. Hebda, J. Pielichowski, Acta Phys. Polon. A 121 (2012) 485–490.
[14] J. Nizioł, H. Harańczyk, J. Kobierski, E. Hebda, J. Pielichowski, B. Ostachowicz, J. Appl. Phys. 114 (2013) 144701.
[15] H. Haranczyk, J. Kobierski, J. Niziol, E. Hebda, J. Pielichowski, D. Zalitacz, M. Marzec, A. El-Ghayoury, J. Appl. Phys. 113 (2013), 044702.
[16] J. Nizioł, P. Nowak, J. Kobierski, H. Harańczyk, Eur. Polym. J. 66 (2015) 301–306.
[17] R.S. Dias, A.A.C.C. Pais, M.G. Miguel, B. Lindman, Colloids Surf. Physicochem. Eng. Aspects 250 (2004) 115–131.
[18] E. Grueso, C. Cerrillos, J. Hidalgo, P. Lopez-Cornejo, Langmuir 28 (2012) 10968–10979.
[19] N. Kobayashi, K. Nakamura, DNA electronics and photonics, in: H. Ishii, K. Kudo, T. Nakayama, N. Ueno (Eds.), Electronic Processes in Organic Electronics: Bridging Nanostructure, Electronic States and Device Properties, Springer Japan, 2015, pp. 253–281.
[20] J. Nizioł, R. Ekiert, J. Kuczkowska, P. Fryń, M. Marzec, Polym. Test. 80 (2019), 106158.
[21] J. Nizioł, J. Fiedor, J. Pagacz, E. Hebda, M. Marzec, E. Gondek, I.V. Kityk, J. Mater. Sci. Mater. Electron. 28 (2017) 259–268.
[22] Y. Shi, X. Li, Org. Electron. 15 (2014) 286–293.
[23] M. Reddeppa, S.B. Mitta, B.-G. Park, S.-G. Kim, S.H. Park, M.-D. Kim, Org. Electron. 65 (2019) 334–340.
[24] P. Stadler, K. Oppelt, T.B. Singh, J.G. Grote, R. Schwodiauer, S. Bauer, H. Piglmayer-Brezina, D. Bauerle, N.S. Sariciftci, Org. Electron. 8 (2007) 648–654.
[25] I. Rau, J.G. Grote, F. Kajzar, A. Pawlicka, Comptes Rendus Physique 13 (2012) 853–864.
[26] T. Suzuki, Y. Kawabe, Opt. Mater. Express 4 (2014) 1411–1419.
[27] A. Pawlicka, F. Sentanin, A. Firmino, J.G. Grote, F. Kajzar, I. Rau, Synth. Met. 161 (2011) 2329–2334.
[28] K. Keren, M. Krueger, R. Gilad, G. Ben-Yoseph, U. Sivan, E. Braun, Science 297 (2002) 72–75.
[29] C.F. Monson, A.T. Woolley, Nano Lett. 3 (2003) 359–363.
[30] R. Seidel, L. Colombi Ciacchi, M. Weigel, W. Pompe, M. Mertig, J. Phys. Chem. B 108 (2004) 10801–10811.
[31] T. Bayrak, N.S. Jagtap, A. Erbe, Int. J. Mol. Sci. 19 (2018) 3019.
[32] U. Nithiyanantham, A. Ramadoss, S.R. Ede, S. Kundu, Nanoscale 6 (2014) 8010–8023.
[33] D.E. Diggs, J.G. Grote, C.M. Bartsch, F. Ouchen, A. Sharma, J.M. Taguenang, A. Kassu, R. Sileshi, Proceedings of the SPIE, 7040 (2008) 70400E-1-6.
[34] R.A. Jones, W.X. Li, H. Spaeth, A.J. Steckl, J. Vacuum Sci. Technol. 26 (2008) 2567–2571.
[35] R. Joksimovic, S. Watanabe, S. Riemer, M. Gradzielski, K. Yoshikawa, Sci. Rep. 4 (2014) 3660.
[36] C. Thibault, V. Le Berre, S. Casimirius, E. Trévisiol, J. François, C. Vieu, J. Nanobiotechnol. 3 (2005) 7.
[37] J. Fredonnet, J. Foncy, S. Lamarre, J.-C. Cau, E. Trévisiol, J.-P. Peyrade, J. M. François, C. Séverac, Microelectron. Eng. 111 (2013) 379–383.
[38] Y. Wang, S.H. Goh, X. Bi, K.-L. Yang, J. Colloid Interface Sci. 333 (2009) 188–194.
[39] E. Bystrenova, M. Facchini, M. Cavallini, M.G. Cacace, F. Biscarini, Angew. Chem. 118 (2006) 4897–4900.
[40] B.D. Myers, Q.-Y. Lin, H. Wu, E. Luijten, C.A. Mirkin, V.P. Dravid, ACS Nano 10 (2016) 5679–5686.
[41] J. Nizioł, K. Makyła-Juzak, A. Radko, R. Ekiert, J. Zemła, N. Górska, A. Chachaj-Brekiesz, M. Marzec, H. Harańczyk, P. Dynarowicz-Latka, Polymer 178 (2019), 121643.
[42] M. Muñoz-Úbeda, S.K. Misra, A.L. Barrán-Berdón, C. Aicart-Ramos, M.B. Sierra, J. Biswas, P. Kondaiah, E. Junquera, S. Bhattacharya, E. Aicart, J. Am. Chem. Soc. 133 (2011) 18014–18017.
[43] D. Janiszek, M.M. Karpinska, A. Niewiadomy, A. Girstun, H. Elzanowska, M. Maj-Zurawska, P.J. Kulesza, Electrochim. Acta 210 (2016) 422–434.
[44] E. Palecek, Crit. Rev. Biochem. Mol. Biol. 26 (1991) 151–226.
[45] M. Munoz-Ubeda, S.K. Misra, A.L. Barran-Berdon, C. Aicart-Ramos, M.B. Sierra, J. Biswas, P. Kondaiah, E. Junquera, S. Bhattacharya, E. Aicart, J. Am. Chem. Soc. 133 (2011) 18014–18017.
[46] J.T. Davies, E.K. Rideal, Interfacial Phenomena, 2 ed., Academic Press, 1963.
[47] G. Roberts (Ed.), Langmuir-Blodgett Films, Springer US, Boston, MA, 1990.
[48] D.K. Chattoraj, K.S. Birdi (Eds.), Adsorption and the Gibbs Surface Excess, Springer US, Boston, MA, 1984.
[49] I. Koltover, T. Salditt, J.O. Rädler, C.R. Safinya, Science 281 (1998) 78–81.
[50] E. Braun, Y. Eichen, U. Sivan, G. Ben-Yoseph, Nature 317 (1998) 775–777.